



Cite this: *Energy Environ. Sci.*, 2021, 14, 6030

Stabilizing electrode–electrolyte interfaces to realize high-voltage Li||LiCoO₂ batteries by a sulfonamide-based electrolyte†

Weijiang Xue, ‡*^a Rui Gao, ^a Zhe Shi, ^{ab} Xianghui Xiao, ^c Wenxu Zhang, ^d Yirui Zhang, ^e Yun Guang Zhu, ^f Iradwikanari Waluyo, ^c Yao Li, ^g Megan R. Hill, ^d Zhi Zhu, ^a Sa Li, ^h Oleg Kuznetsov, ⁱ Yiman Zhang, ⁱ Wah-Keat Lee, ^c Adrian Hunt, ^c Avetik Harutyunyan, ⁱ Yang Shao-Horn, *^{bef} Jeremiah A. Johnson *^d and Ju Li *^{ab}

High-voltage lithium-metal batteries (LMBs) with LiCoO₂ (LCO) as the cathode have high volumetric and gravimetric energy densities. However, it remains a challenge for stable cycling of LCO > 4.5 V_{Li}. Here we demonstrate that a rationally designed sulfonamide-based electrolyte can greatly improve the cycling stability at high voltages up to 4.7 V_{Li} by stabilizing the electrode–electrolyte interfaces (EEIs) on both the Li-metal anode (LMA) and high-voltage LCO cathode. With the sulfonamide-based electrolyte, commercial LCO cathodes retain 89% and 85% of their capacities after 200 and 100 cycles under high charging voltages of 4.55 V_{Li} and 4.6 V_{Li}, respectively, significantly outperforming traditional carbonate-based electrolytes. The surface degradation, impedance growth, and detrimental side reactions in terms of gas evolution and Co dissolution are well suppressed. Our work demonstrates a promising strategy for designing new electrolytes to realize high-energy Li||LCO batteries.

Received 27th April 2021,
Accepted 27th September 2021

DOI: 10.1039/d1ee01265g

rsc.li/ees

Broader context

The demand for higher energy density (e.g. > 400 W h kg⁻¹) urges us to explore more aggressive chemistries beyond traditional lithium-ion batteries (LIBs), including high-voltage LiCoO₂ (LCO) cathodes and lithium-metal anodes. However, such chemistries are usually accompanied by high electrochemical reactivity and unstable electrode–electrolyte interfaces (EEIs), making it challenging to maintain a satisfactory cycle life. In the present work, we demonstrate that our sulfonamide-based electrolyte effectively stabilizes the EEIs and thus enables excellent cycling performance of the 4.5–4.7 V_{Li} LCO||Li-metal batteries. By employing several *in situ* and *ex situ* techniques, the oxidative stability of the sulfonamide-based electrolyte and the evolution of the EEIs on LCO surfaces at different potentials were studied, revealing the role of electrolytes in stabilizing the LCO single-crystal surfaces and in preventing intragranular stress corrosion cracking (SCC).

Lithium-ion batteries (LIBs) have conquered important markets of electric vehicles, portable electronics, and robotics due to their high energy density/efficiency and long cycle life.¹ The significant growth in the demand for higher energy

density^{2,3} (e.g. > 400 W h kg⁻¹) urges us to explore more aggressive chemistries beyond traditional LIBs, including high-voltage-capacity cathodes and conversion-type anodes. However, such chemistries are usually accompanied by high

^a Department of Nuclear Science and Engineering, Massachusetts Institute of Technology, Cambridge, Massachusetts 02139, USA. E-mail: xuewj@mit.edu, lju@mit.edu

^b Department of Materials Science and Engineering, Massachusetts Institute of Technology, Cambridge, Massachusetts 02139, USA. E-mail: shaohorn@mit.edu

^c National Synchrotron Light Source II, Brookhaven National Laboratory, Upton, NY 11973, USA

^d Department of Chemistry, Massachusetts Institute of Technology, Cambridge, Massachusetts 02139, USA. E-mail: jaj2109@mit.edu

^e Department of Mechanical Engineering, Massachusetts Institute of Technology, Cambridge, Massachusetts 02139, USA

^f Research Laboratory of Electronics, Massachusetts Institute of Technology, Cambridge, MA 02139, USA

^g State Key Lab of Metal Matrix Composites, Shanghai Jiao Tong University, Shanghai 200240, China

^h Institute of New Energy for Vehicles, School of Materials Science and Engineering, Tongji University, Shanghai, 201804, China

ⁱ Honda Research Institute, USA, Inc., San Jose, California 95134, USA

† Electronic supplementary information (ESI) available. See DOI: 10.1039/d1ee01265g

‡ These authors contributed equally to this work.



electrochemical reactivity and unstable electrode–electrolyte interfaces (EEIs), making it challenging to maintain a satisfactory cycle life.⁴ Therefore, it is crucial to form stable EEIs to mitigate the degradation of reactive electrodes and electrolytes.

For the cathode, an effective approach to increase the energy output is to extend the operating voltages, especially for LiCoO_2 (LCO), the dominant cathode in current LIBs for consumer electronics^{5,6} because of its superior volumetric energy density (E_v). However, the charging voltage in commercial products⁷ is usually limited below 4.35 V_{Li}, yielding a discharge capacity of $\sim 165 \text{ mA h g}^{-1}$ ($\text{Li}_{1-x}\text{CoO}_2$, $x = \sim 0.6$), still far away from the theoretical maximum (274 mA h g⁻¹), because the substantial increase in capacity achieved at higher charging cut-off voltage ($\geq 4.5 \text{ V}_{\text{Li}}$) would come at the expense of rapid decay of capacity and efficiency.⁸ For high-voltage LCO, constructing a stable cathode–electrolyte interface (CEI) is challenging due to the high reactivity between electrolyte components and high-valence Co^{2+} ($\alpha > 3$) / O^{2-} ($\beta < 2$).^{9,10} On the one hand, the undesirable electrolyte decomposition¹¹ including solvent oxidation and hydrogen abstraction¹² from solvent molecules leads to the formation of high-impedance CEIs generally in the form of oxyfluorides/oligomers.¹³ On the other hand, the parasitic electrolyte–cathode reaction promotes further degradation, including the formation of ionically resistive spinel¹⁴ transformed from the layered structure, Co dissolution in the electrolyte^{15,16} and O loss¹⁷ from oxygen evolution. Therefore, constructing stable CEIs to mitigate these degradations is required. Prevailing strategies for protecting LCO are bulk doping^{7,8,18} and surface modification.^{5,9,15,17,19–23} An alternative strategy is to develop highly compatible electrolytes to form stable CEIs. Although fluorinated electrolytes,^{24,25} multifunctional polymer electrolyte,^{26,27} and additives^{28,29} have demonstrated promising cyclability improvement, such explorations have been focused mainly on charging voltages up to 4.5 V_{Li}^{24,25,30} (Table S1, ESI†). It still remains challenging to design suitable electrolytes for higher-voltage ($> 4.5 \text{ V}_{\text{Li}}$) LCO.

For the anode, the lithium-metal anode^{31–33} (LMA) has become a hot topic in recent years due to its highest theoretical capacity of 3861 mA h g⁻¹ (ten times that of the commercial graphite anode, 374 mA h g⁻¹). However, significant challenges associated with the instability of LMA still hinder the practical application of lithium-metal batteries (LMBs).³³ Unstable solid-electrolyte interface (SEI) between reactive Li and electrolyte³⁴ leads to severe side reactions, detrimental deposition morphology like mossy Li, and thus poor LMA reversibility. To realize highly reversible LMBs, therefore, the key is to construct stable LMA–electrolyte interfaces, which again calls for developing reliable electrolytes.³⁵

In order to simultaneously achieve stable EEIs on both LCO and LMA to increase cycling stability at high voltages $> 4.5 \text{ V}_{\text{Li}}$, we have taken a molecular design approach utilizing stable functional groups that mimic the structures of common Li-salt anions.³⁶ Using this strategy, we recently discovered a new class of sulfonamide electrolytes based on *N,N*-dimethyltrifluoromethanesulfonamide^{37–39} (DMCF₃SA) to enable stable cycling of $\text{LiNi}_{0.8}\text{Co}_{0.1}\text{Mn}_{0.1}\text{O}_2$ (NMC811) at an ultrahigh charging voltage of 4.7 V_{Li}.³⁹ In such

an agglomerated polycrystalline cathode, oxidative dehydrogenation of carbonate solvents to generate protic species^{12,40,41} and intergranular cracking⁴² are mainly responsible for the performance degradation using traditional electrolytes because they lead to the loss of electronic contact and more parasitic reactions between the exposed surfaces of the primary particle grains and the electrolyte infiltrating along the intergranular cracks. Our sulfonamide-based electrolyte is chemically stable against oxidative dehydrogenation, which effectively stabilizes the grain boundaries (GB) under cyclic stress by relieving the chemical dissolution attack and thus suppressing the GB cracking. But the situation with the LCO cathode is arguably quite different. Industrially, LCO is typically made using a solid-state synthesis method, producing large single crystals on the order of ten microns, that can be hard-rolled into electrodes to improve the electrode density, whereas NMC is typically made with wet co-precipitation methods with complex primary/secondary-particle structures, that are known to be quite fragile and cannot be hard-rolled in electrode manufacturing. Thus, the starting microstructures are quite different, and therefore the stress-corrosion cracking (SCC) pathway due to the electrolyte corrosion and phase-transformation stress could be quite different between NMC and LCO electrodes. Also, investigations on electrolyte interactions with the cathode primary particle, especially with the more reactive surfaces than NMC's (such as LCO surface), as well as the correlation with the electrochemical performance are still missing, which are critical for understanding not only the sulfonamide-based-electrolyte–cathode interaction but also the broader cathode degradation mechanisms.

In this work, single-crystalline LCO particles, which can exhibit high surface reactivity towards oxidative dehydrogenation of carbonate solvents,⁴³ is selected in the present work. By employing several *in situ* and *ex situ* techniques, the oxidative stability of the sulfonamide-based electrolyte (1 M LiFSI in DMCF₃SA) and the evolution of the CEIs on LCO surfaces at different potentials were studied, revealing the role of electrolytes in stabilizing the LCO single-crystal surfaces. This sulfonamide-based electrolyte greatly improves the cycling performance of commercial LCO cathodes at high charging voltages of 4.5 V_{Li} to 4.7 V_{Li} by suppressing the LCO surface degradation and side reactions. In particular, with the sulfonamide-based electrolyte, LCO cathodes demonstrate high capacity retentions of 89% and 85% under 4.55 V_{Li} and 4.6 V_{Li} with excellent Coulombic efficiencies (CE $\sim 99.84\%$) and rate performance, respectively. Compared to our work on NMC811³⁹ with an $E_v \sim 3100 \text{ W h L}^{-1}$, the present 4.6 V_{Li} LCO exhibits much higher $E_v > 3600 \text{ W h L}^{-1}$ with comparable cycling stability. The sulfonamide-based electrolyte also enables a high CE $\sim 99.7\%$ for Li stripping/plating on a Li matrix. Post-cycling microstructural evaluation revealed suppressed intragranular cracking in high-voltage LCO, instead of suppressed intergranular cracking in NMC. Our work highlights the importance of constructing stable EEIs against SCC and provides a new approach for designing new electrolytes for high-voltage LMBs.

In this work, we selected 1.2 M LiPF₆ in ethylene carbonate (EC)/ethyl methyl carbonate (EMC) (3 : 7 wt%) as the reference electrolyte (Fig. S1, ESI†). To evaluate the oxidation stability of



different solvents, we employed density functional theory (DFT) calculations to compare the energetics of oxidation reactions ΔE between EC/DMCF₃SA molecules and the highly delithiated LCO surface⁴⁰ (Fig. 1a and b). Note that EC dissociation ($\Delta E_{EC} = -3.02$ eV) is energetically more favorable than DMCF₃SA dissociation ($\Delta E_{DMCF_3SA} = -2.87$ eV), implying a higher oxidation resistance of the latter molecule. Experimentally, linear sweeping voltammetry (LSV) was used with Al foil as the working electrode. Fig. 1c shows that the onset of oxidation in the sulfonamide-based electrolyte is ~ 5 V_{Li} with no peak corresponding to Al corrosion,³⁹ while the oxidation of the carbonate-based electrolyte starts at ~ 4.2 V_{Li}.⁴⁴ The excellent oxidation resistance and compatibility with the Al current collector of the sulfonamide-based electrolyte are essential for operating the LCO cathode at high voltages.

Three types of commercial LCO cathodes were tested. The S-LCO, A-LCO, and T-LCO denote the LCO purchased from Sigma Aldrich without any doping or coating, the one provided by Argonne National Lab, and the one purchased from Targray Co, respectively. The electrochemical performances of all Li||LCO batteries were evaluated using galvanostatic cycling with charging voltages from 4.5 V_{Li} to 4.7 V_{Li} at room temperature. With our sulfonamide-based electrolyte, the uncoated and undoped S-LCO exhibits significantly increased capacity retention

of 91% and 79% at 4.5 V_{Li} and 4.55 V_{Li}, compared to 24% and 5% with the carbonate-based electrolyte after 200 cycles, respectively (Fig. S2, ESI[†]). It indicates that the CEI stability plays a dominant role in the capacity fading at 4.5 V_{Li}⁴⁶ rather than the bulk stability because excellent cycling stability can be achieved by choosing a more reliable electrolyte without the assistance from LCO doping or coating (Fig. S3, ESI[†]). We also evaluated the commercial A-LCO cathode, which should have been doped as the minor peaks⁴⁷ at 4.1–4.2 V_{Li} in the voltage profiles of the undoped S-LCO (indicated by the red circles in Fig. S2b, c, e and f, ESI[†]) associated with order-disorder transitions are eliminated.⁷ Under a charging voltage of 4.5 V_{Li} and a discharge rate of 150 mA g⁻¹, the Li||A-LCO cell with the carbonate-based electrolyte exhibits very low capacity retention of 7%, a low operating mid-voltage retention of $\sim 81.00\%$ and an average CE of $\sim 99\%$ after 200 cycles (Fig. 2a–c). The voltage profiles in Fig. S4 (ESI[†]) indicate obvious overpotential growth during cycling. In contrast, the 4.55 V_{Li} cycling performance of the Li||A-LCO cell with the sulfonamide-based electrolyte is dramatically improved. The cell shows an initial capacity of 200.8 mA h g⁻¹ with 89% and 99.74% retention of the capacity and operating mid-voltage after 200 cycles (Fig. 2a and c), respectively. An excellent average CE of $\sim 99.84\%$ (Fig. 2b) suggests that the undesired side reactions between the A-LCO cathode and electrolyte are largely suppressed. Even at a higher

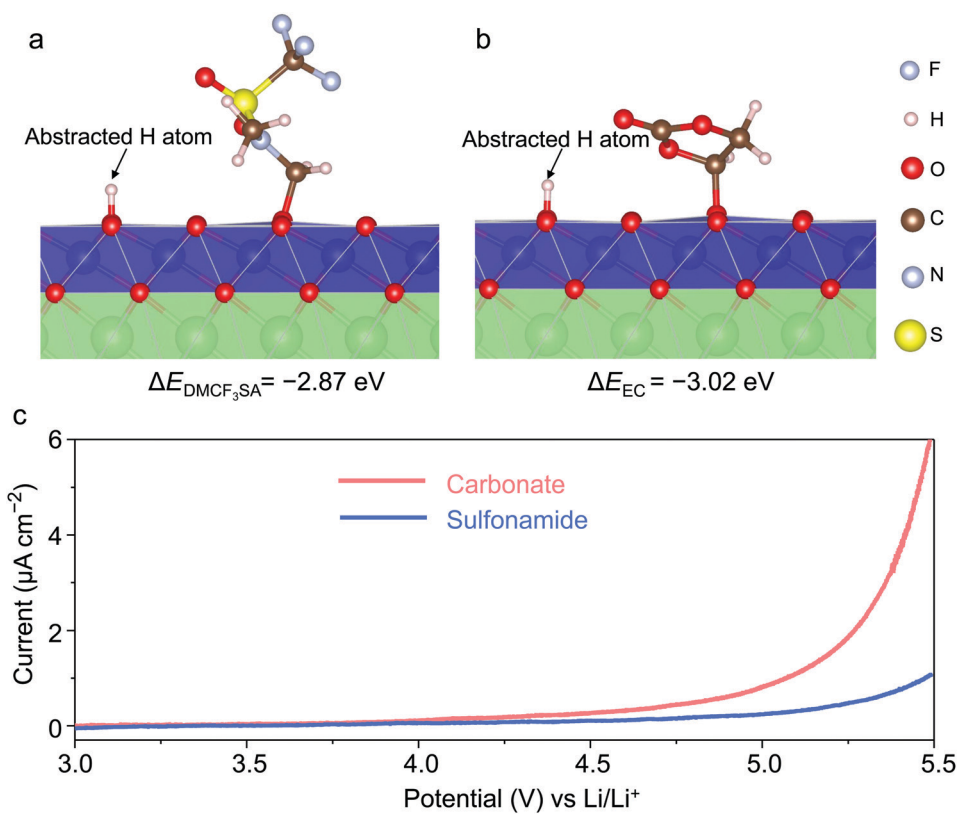


Fig. 1 Electrolyte design and performance. Relaxed structure and reaction energy ΔE of DMCF₃SA (a) and EC (b) oxidized by the highly delithiated LCO surface, as determined from DFT calculations. The reaction energies are -2.87 eV for DMCF₃SA and -3.02 eV for EC, respectively. The reaction on the LCO surface includes H-abstraction and C–O bond formation between the solvent and the LCO.^{41,43,45} (c) Oxidation stability of different electrolytes evaluated by linear sweeping voltammetry at a scanning rate of 4 mV s⁻¹. The sulfonamide-based and carbonate-based electrolytes are 1 M LiFSI in DMCF₃SA and 1.2 M LiPF₆ in EC/EMC (3 : 7 wt%), respectively.



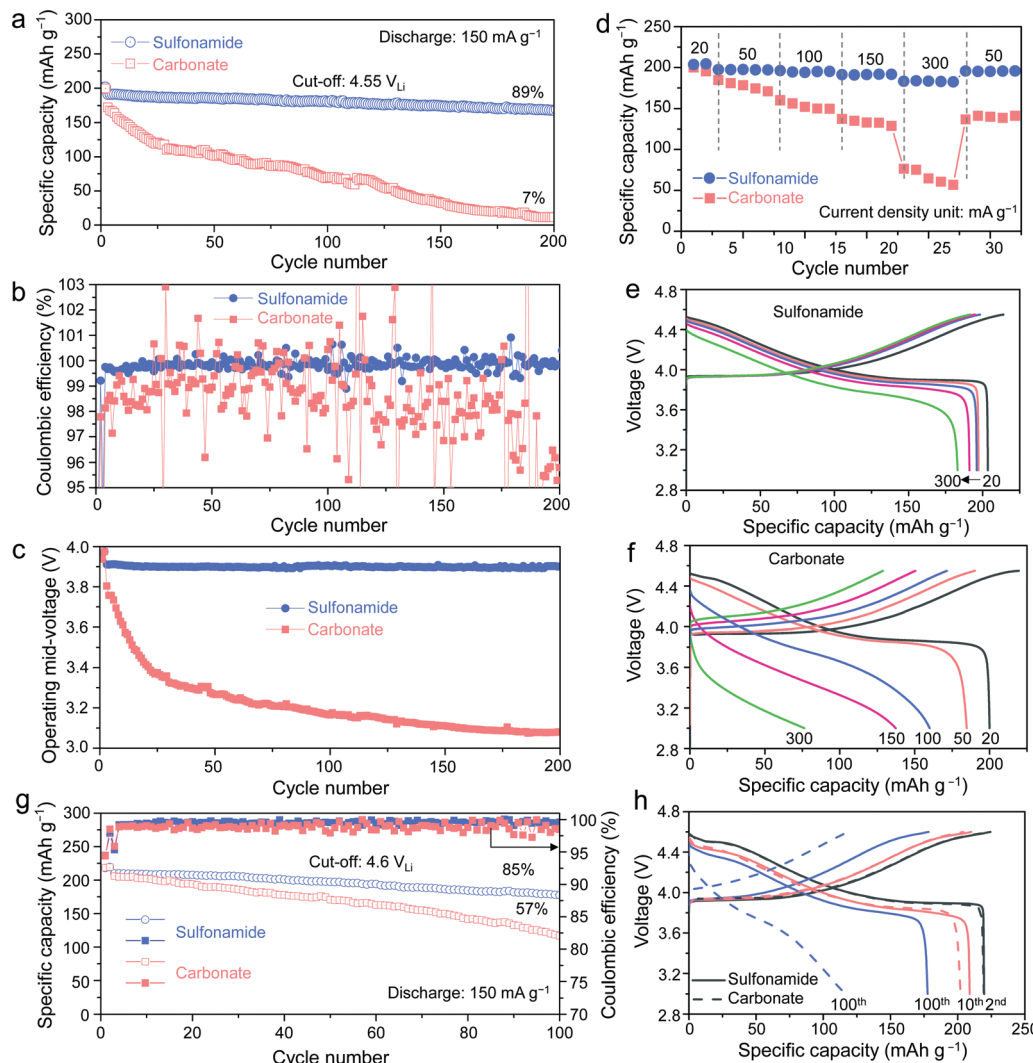


Fig. 2 Electrochemical performance of Li||LCO cells with different electrolytes. The specific capacities (a), Coulombic efficiencies (b), and operating mid-voltages (c) of Li||A-LCO cells as a function of cycle number with different electrolytes. The upper charging voltage was 4.55 V_{Li}. The current densities during charging and discharging were 50 mA g⁻¹ and 150 mA g⁻¹, respectively. 10 mA g⁻¹ charging–discharging was used for the initial 1st cycle. (d) Rate performance of Li||A-LCO cells at 4.55 V_{Li} and corresponding voltage profiles with the sulfonamide (e) and carbonate (f) electrolytes. The unit of the current densities in (d–f) is mA g⁻¹. (g) Cycling performance of Li||T-LCO cells and the corresponding voltage profiles (h) at a charging voltage of 4.6 V_{Li} and current densities of 50 mA g⁻¹ for charging and 150 mA g⁻¹ for discharging at room temperature. 10 mA g⁻¹ charging–discharging was used for the initial two cycles. The amounts of the sulfonamide-based and carbonate-based electrolytes were ~15 µL and ~50 µL per cell, respectively. 350-µm-thick Li foils were used.

charging voltage of 4.6 V_{Li}, our electrolyte shows enhanced cycling stability (Fig. S5, ESI[†]) with a high cathode-specific $E_v > 3600 \text{ W h L}^{-1}$. Despite the poor LMA compatibility of the carbonate-based electrolyte, under our testing conditions, including superabundant LMA and electrolyte, the LMA does not affect the cycling performance (Fig. S6, ESI[†]), which allows systematic comparison of all cathode performances with both electrolytes.

Besides investigating the electrolyte effect on the cycling stability, the rate performance at 4.55 V_{Li} was also evaluated (Fig. 2d–f). The Li||A-LCO cell using the sulfonamide-based electrolyte exhibits higher reversible capacities of 197.3 mA h g⁻¹, 196.1 mA h g⁻¹, 191.2 mA h g⁻¹, and 183.1 mA h g⁻¹ compared to 184.7 mA h g⁻¹, 160.0 mA h g⁻¹, 137.4 mA h g⁻¹, and 76.4 mA h g⁻¹ with the reference electrolyte at current density of 50 mA g⁻¹ to 300 mA g⁻¹, respectively. The excellent rate performance at

high voltages is also a good indicator of the stable CEI and LCO surface. Furthermore, another commercial T-LCO cathode was also evaluated at higher charging voltages of 4.6–4.7 V_{Li}. Although the Li||T-LCO cells with both electrolytes reach similar high initial capacities ~220 mA h g⁻¹, the capacity retentions show a dramatic difference (85% vs. 57%, Fig. 2g and h). For 4.65 V_{Li} and 4.7 V_{Li}, the sulfonamide-based electrolyte enables high initial capacities of 227.2 mA h g⁻¹ and 241.5 mA h g⁻¹ with greatly improved cycling stability compared to the carbonate-based electrolyte (Fig. S7, ESI[†]). Furthermore, our electrolyte demonstrates excellent cycling stability (4.55 V_{Li}, 97.6% capacity retention, CE ~99.88% after 70 cycles, Fig. S8, ESI[†]) at a high temperature of 45 °C.

To shed light on the degradation mechanisms, the following investigations are focused on A-LCO cathodes after cycling at

4.55 V_{Li} in different electrolytes. We first conducted the galvanostatic intermittent titration technique (GITT) on the Li||A-LCO cells to measure the impedance growth after cycling (Fig. 3a and b). For the reference electrolyte, severe impedance growth and huge overpotentials after 200 cycles are observed (Fig. 3b, average overpotential is 758 ± 80 mV). In comparison, for our electrolyte, the overpotentials are an order of magnitude smaller after 200 cycles (Fig. 3b, average overpotential is 15 ± 4 mV), which is consistent with the better capacity retention and rate capability reported above. Such a prominent difference in the overpotential growth by using different electrolytes can also be supported by electrochemical impedance spectroscopy (EIS) measurements. For the A-LCO with the carbonate-based electrolyte, cycling at 4.55 V_{Li} induced a much higher charge

transfer resistance (R_{ct}) than the one cycled in the sulfonamide-based electrolyte (Fig. S9, ESI†). The continuous impedance growth hinders the bulk from achieving a high oxidation state and thus leads to a large difference in the Co oxidation states in the cycled A-LCO cathodes, which was revealed by the X-ray absorption near edge structure (XANES) mode of full-field X-ray imaging (FXI). Co oxidation states were mapped by tracking the whiteline peak positions⁴⁸ of the XANES spectra acquired by scanning every pixel ($\sim 20 \times 20 \text{ nm}^2$ area) in a $40 \times 40 \mu\text{m}^2$ area of interest (Fig. 3c and d). After charging the cycled A-LCO cathodes to 4.55 V_{Li}, higher and more uniform Co valences are noted in the one cycled with our electrolyte (Fig. 3c) than that with the carbonate-based electrolyte (Fig. 3d). This result is further confirmed by the plotted

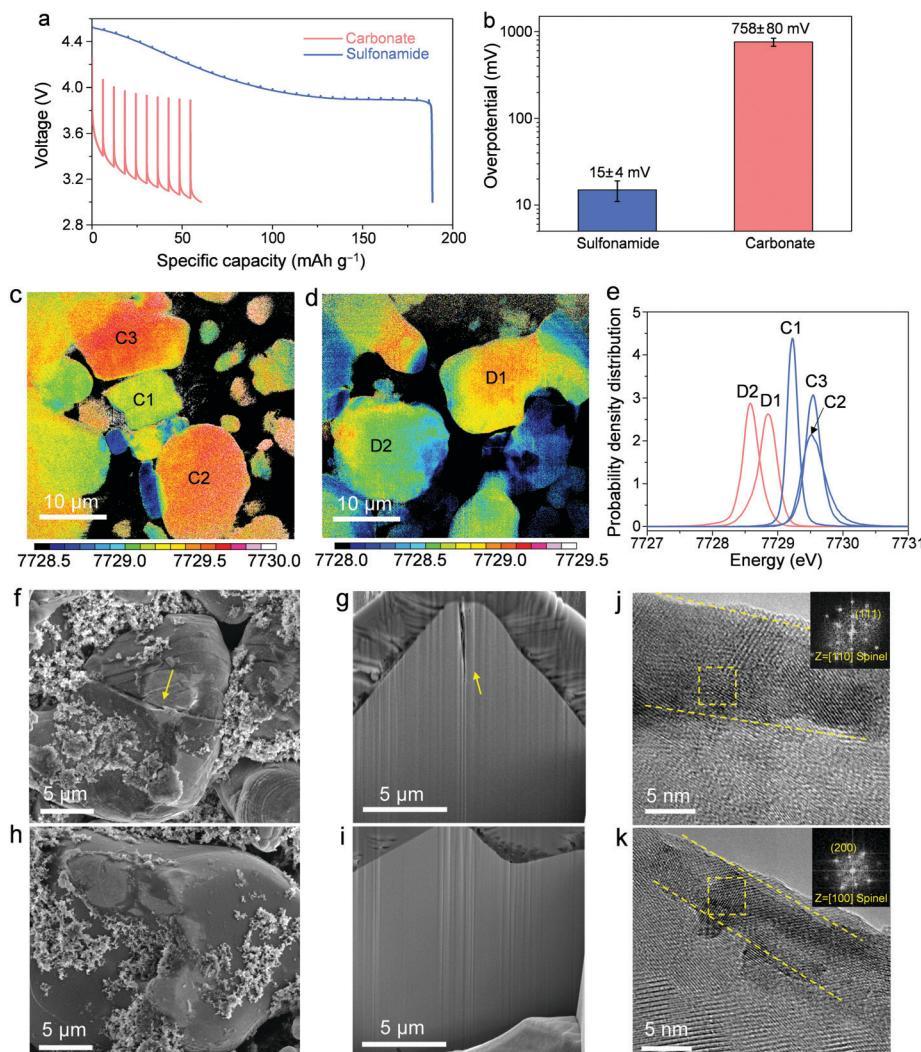


Fig. 3 Characterization of the A-LCO cathodes cycled in different electrolytes at 4.55 V charging voltage. (a) Discharge voltage profiles from GITT plots of the cells after 200 cycles in different electrolytes. (b) Average overpotentials over different discharge states with error bars for standard deviation. XANES mapping of the A-LCO particles cycled in the sulfonamide-based (c) and carbonate-based (d) electrolytes for 100 cycles and then charged to 4.55 V_{Li}. Statistical analysis (e) of the whiteline distributions of particles in c and d. All the C1, C2, and C3 particles with the sulfonamide-based electrolyte have higher Co oxidation states than D1 and D2 particles with the carbonate-based electrolyte. SEM images of the surfaces (f and h), the cross-sections (g and i), and HRTEM images (j and k) of A-LCO cathodes after 200 cycles in the carbonate-based (f, g and j) and sulfonamide-based (h, i and k) electrolytes. Yellow dot lines in (j and k) indicate the transformed spinel layers. Insets in (j and k) in the upper right corners are the FFT patterns from the areas indicated by the yellow squares, indicating that the transformed layers are spinel structures.



histograms of the whiteline distributions of several representative particles (Fig. 3e).

We investigated the microstructure and surfaces to understand the origin of impedance growth.²⁰ Post-cycling analysis was conducted on the surfaces and cross-sections by scanning electron microscopy (SEM, Fig. 3f-i and Fig. S10, ESI[†]). As highlighted by yellow arrows in Fig. 3f and g, the A-LCO cycled in the carbonate-based electrolyte shows apparent cracks in the bulk particle while the one cycled in the sulfonamide-based electrolyte keeps intact (Fig. 3h and i). This result suggests that the SCC behavior usually observed in polycrystalline NMC cathodes³⁹ is also present in the deep-cycled LCO cathode with a single-crystalline microstructure, which is usually considered not to crack easily.⁴⁹ Similar cracking behavior was previously reported in deep-cycled single-crystalline NMC⁵⁰ and LCO^{7,24} cathodes. Considering the high catalytic capability of the LCO surface that may promote more intensive side reactions, a “good” electrolyte or proper surface modification that can passivate the surface cracks and thus suppress the SCC, is required for > 4.5 V_{Li} LCO.

Another surface degradation causing impedance growth and slow charge transfer kinetics is the surface transformation from the original layered structure to spinel phase,⁵¹ resulting from the reduction of high-valence Co²⁺ by electrolyte components. A visible difference in the thickness of the detrimental layers is identified by high-resolution transmission electron microscopy (HRTEM). While the resistive layer is ~ 11 nm thick (Fig. 3j) for the A-LCO cycled in the carbonate-based electrolyte, it is suppressed by our sulfonamide-based electrolyte (~ 5 nm thick, Fig. 3k). Fast Fourier transform (FFT) patterns in the insets of Fig. 3j and k show that the detrimental layers are spinel phases. Consistently, higher-degree cation-mixing in the bulk structure of the A-LCO cycled in the carbonate-based electrolyte is revealed by a decrease in the intensity ratio of I_{003}/I_{104} in the XRD pattern compared to the one cycled in the sulfonamide-based electrolyte (Fig. S11, ESI[†]). These results indicate that our electrolyte greatly mitigates the surface degradation and thus suppresses the resultant impedance growth at high charging voltages, which is consistent with the improved cycling performance in Fig. 2.

The differences in the surface and interface degradation are mainly attributed to the cathode–electrolyte side reactions, as will be investigated by characterizing the side reaction byproducts in terms of gas emission, CEI, and Co dissolution. Differential electrochemical mass spectroscopy (DEMS) was carried out to monitor the gas evolution during charging to 4.7 V_{Li}. When A-LCO is charged to above 4.5 V_{Li} in the carbonate-based electrolyte, obvious CO₂ gas begins to release (Fig. 4a), confirming the oxidation of electrolyte components. In contrast, no obvious gaseous products including CO₂, O₂ (Fig. 4b), or other possible gases (Fig. S12, ESI[†]) are detected with the sulfonamide-based electrolyte, demonstrating its excellent oxidation resistance.

In order to shed more light on the oxidation process of our sulfonamide-based electrolyte on LCO surfaces, first, *in situ* Fourier-transform infrared spectroscopy (FT-IR)¹² was

performed to characterize the evolution of CEIs during galvanostatic charging to 4.8 V_{Li}. Upon charging LCO from open circuit potential (OCP) to 4.8 V_{Li} (Fig. 4c), obvious changes in the IR spectra are observed from 3.9 V_{Li} to 4.2 V_{Li} (Fig. 4d). A peak at ~ 1260 cm⁻¹ in the S=O region, which appeared the earliest at ~ 4.0 V_{Li}, was noted. It could be attributed to the decomposition of LiFSI or DMCF₃SA since they both have S=O groups. Upon further charging from 4.2 V_{Li} to 4.8 V_{Li}, the spectra almost remain unchanged (Fig. 4d), indicating good chemical stability of the CEIs against oxidation, which can be further confirmed by the unchanged spectra acquired during holding the potential at 4.8 V_{Li} and subsequent resting at OCP (Fig. S13, ESI[†]).

Second, an *ex situ* X-ray photoelectron spectrometer (XPS) was used to analyze the surface chemistry of the carbon-free, binder-free electrodes at different states of charge in our sulfonamide-based electrolyte, which can avoid interference from the binder and high-surface-area conductive carbon.¹³ Solvent oxidation on LCO surfaces upon charging to ~ 4.4 V_{Li} is confirmed by XPS analysis of C 1s (Fig. 4e) as the peak intensities at high binding energies (*i.e.*, corresponding to oxidized carbon such as C–O and C–SO_x) increase from 4.2 V_{Li} to 4.4 V_{Li}, indicating the growth of surface species formed by DMCF₃SA decomposition. Above 4.4 V_{Li}, the C 1s spectra remain almost unchanged with increasing voltage, suggesting a good CEI stability at high voltages, which matches well with the FT-IR results in Fig. 4d. On the other hand, S–F species are noted from F 1s spectra (Fig. 4f) from 4.4 V_{Li} and above, which is likely attributed to the decomposition of LiFSI salt with the S–F bond rather than the DMCF₃SA solvent with the CF₃ bond. The higher C–F peak intensity than the S–F one (Fig. 4f) implies that the CEIs on the LCO surface are mainly derived from the decomposition of DMCF₃SA solvent rather than LiFSI salt.

In addition, the A-LCO cathodes after cycling in different electrolytes were also examined by XPS and soft X-ray absorption spectroscopy (sXAS). The CEI formed in the reference electrolyte is mainly composed of solvent decomposition products as evidenced by the C–O, C=O,^{52,53} and CO₃²⁻ species,²⁴ while less are observed for that formed in the sulfonamide-based electrolyte (Fig. S14a, S15a and S15b, ESI[†]). Note that the presence of these carbon–oxygen species usually correlates with the dehydrogenation of carbonate molecules¹³ and the resultant formation of corrosive HF.²⁴ A LiF-rich CEI formed in the sulfonamide-based electrolyte is also noted in the F K-edge sXAS spectra²⁴ (Fig. S15c and d, ESI[†]), which is believed to be a favorable feature for enhancing the cathode stability.^{32,44,54} Another difference in CEI components lies in the N and S induced by the sulfonamide-based electrolyte (Fig. S16, ESI[†]), which is absent in the CEI formed in the carbonate-based electrolyte. Furthermore, suppressed Co dissolution by the sulfonamide-based electrolyte is revealed by the Co 2p XPS results (Fig. S14c, ESI[†]). It is likely that the less Co dissolution can be attributed to the formation of stable CEI, which can effectively suppress side reactions between the electrolyte and LCO and thus prevent the Co species from leaching out from the



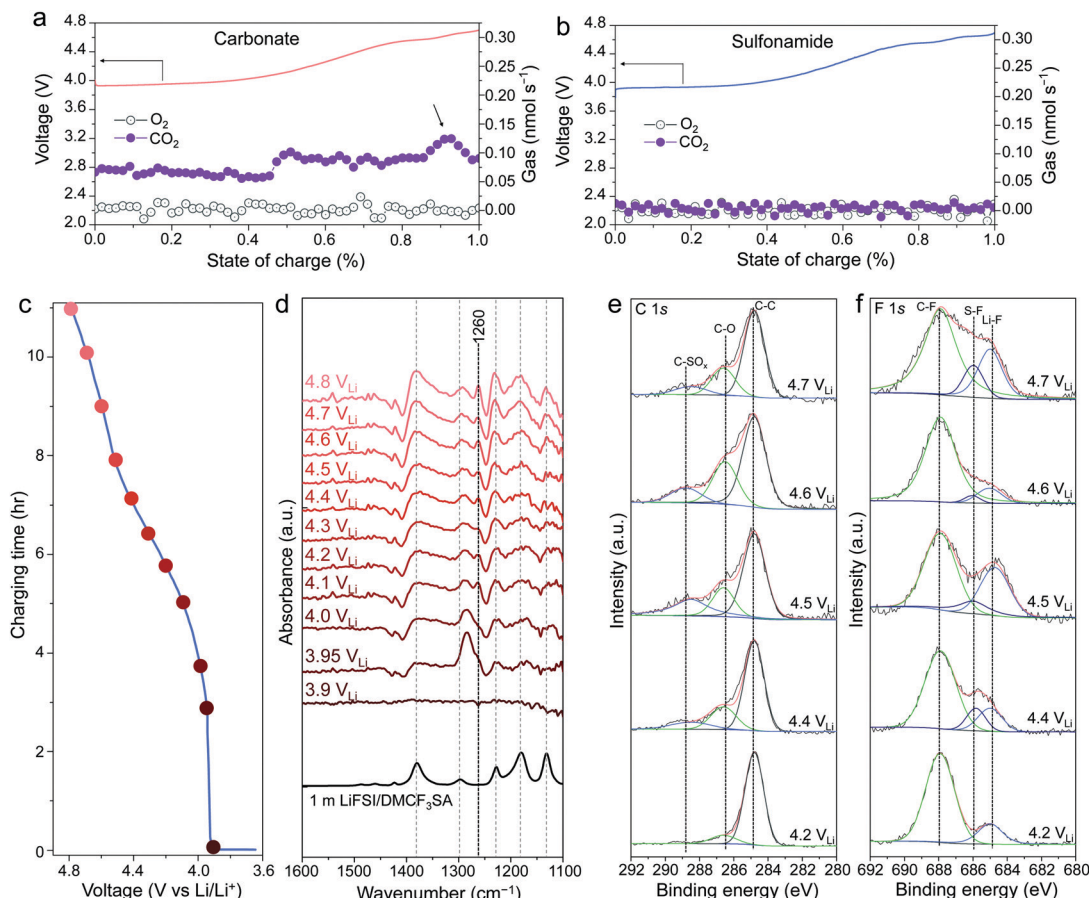


Fig. 4 Characterization of the cathode-electrolyte side reaction and the surface chemistry of CEIs of the LCO cathodes. *In situ* DEMS analysis of the gas evolution during first charging in the carbonate-based (a) and sulfonamide-based (b) electrolytes. (c) Voltage profile of LCO during charging to $4.8 \text{ V}_{\text{Li}}$ in the sulfonamide-based electrolyte. (d) *In situ* FT-IR spectra on LCO surfaces upon charging to $4.8 \text{ V}_{\text{Li}}$ in the sulfonamide-based electrolyte. XPS spectra of the C 1s (e) and F 1s (f) for the carbon-free, binder-free LCO electrodes after charging to 4.2, 4.4, 4.5, 4.6, and $4.7 \text{ V}_{\text{Li}}$ with the sulfonamide-based electrolyte.

cathode. These results clearly manifest that transition-metal cation dissolution is greatly suppressed and a stable CEI is thus constructed in our sulfonamide-based electrolyte, which benefits the high-voltage electrochemical performance.

In addition to stabilizing the high-voltage LCO cathodes, it is also very important for an electrolyte to have good compatibility with the LMA to realize long-term cycling stability in $\text{Li}||\text{LCO}$ batteries. Although our electrolyte has shown good compatibility with LMA,³⁹ the CE evaluated by $\text{Li}||\text{Cu}$ configuration is more appropriate to correlate with an “anode-free” scenario, which is not applicable for our $\text{Li}||\text{LCO}$ batteries with excess Li inventory. Therefore, we adopted another well-established method⁵⁵ by $\text{Li}||\text{Li}$ configuration to evaluate the Li-metal stripping/plating CE on the Li matrix (Fig. 5a). Our sulfonamide-based electrolyte shows a much higher CE $\sim 99.7\%$ and smaller overpotentials during Li plating and stripping than the carbonate-based electrolyte (CE $\sim 65.7\%$). The significant difference in CE can be mainly attributed to Li metal morphologies and SEIs formed in different electrolytes. To investigate the LMA morphology, LMAs were retrieved from the $\text{Li}||\text{A-LCO}$ cells after 100 cycles in different electrolytes at $4.55 \text{ V}_{\text{Li}}$. Dendrite-like Li deposits are

seen on the LMA cycled in the carbonate-based electrolyte (Fig. 5b). Such a high-surface-area morphology can promote the harmful side reactions between the LMA and electrolyte, thus leading to poor LMA reversibility.⁵⁴ In addition, an obvious Co signal from the electron dispersive spectroscopy (EDS) spectrum (Fig. 5c) is detected, which is believed to have migrated from the LCO cathode, matching well with the cathode result in Fig. S14c (ESI[†]). In contrast, with our sulfonamide-based electrolyte, the morphology of Li deposits tends to be large particles with less surface area (Fig. 5d) without the presence of crossover Co (Fig. 5e), which is desirable for LMA reversibility. Furthermore, we evaluated the electrolyte by an anode-free A-LCO||Cu cell under lean electrolyte conditions. Our electrolyte successfully enables capacity retention as high as 72% after 70 cycles (Fig. S17, ESI[†]), indicative of its excellent compatibility with both the LMA and high-voltage LCO cathode.

Furthermore, to understand the effects of both electrolytes on the SEIs, surface chemistry analysis by XPS was conducted on the cycled LMAs. Since carbon-containing species are mainly derived from the electrolyte solvents, we can trace C 1s to get more information on the solvent decomposition on LMAs.



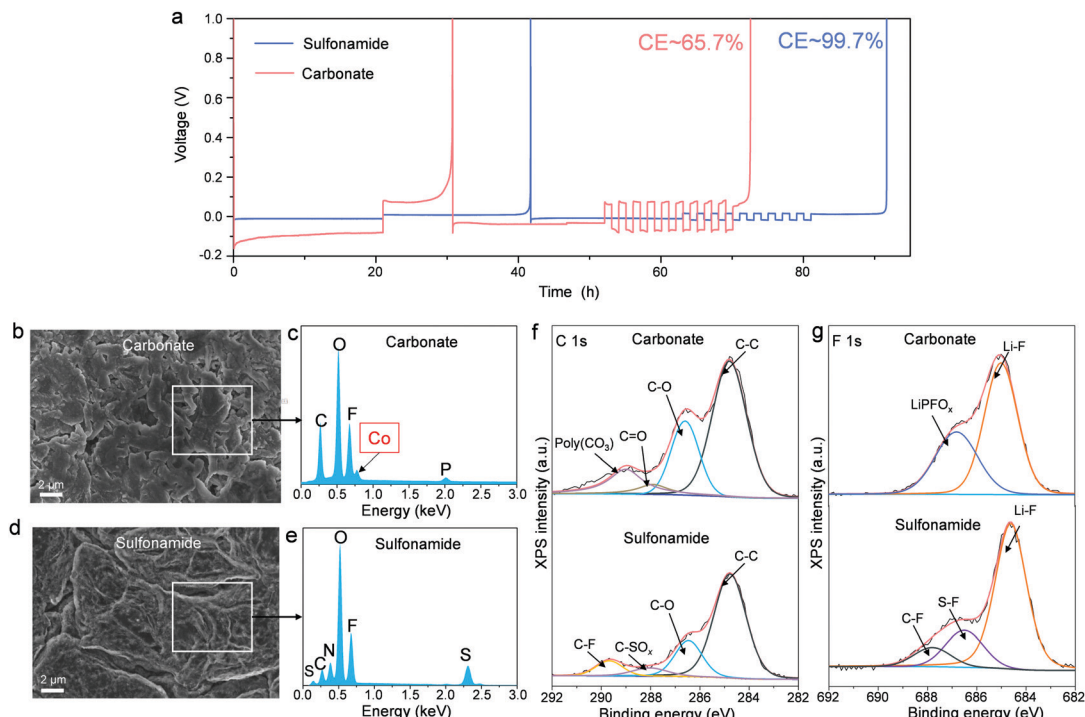


Fig. 5 Electrochemical performance and characterization of the LMAs in different electrolytes. (a) Li-metal stripping/plating CEs in the sulfonamide-based and carbonate-based electrolytes. SEM figures and corresponding elemental analysis by EDS of the LMAs extracted from the Li||A-LCO cells after 100 cycles at 4.55 V_{Li} in the carbonate-based (b and c) and sulfonamide-based (d and e) electrolytes. XPS spectra of C K-edge (f) and F K-edge (g) of the A-LCO cathodes cycled in different electrolytes.

The lower C 1s intensity in Fig. 5f indicates less solvent decomposition for the sulfonamide than carbonates. In addition, the F 1s XPS spectra (Fig. 5g) reveal that the LiF content in the SEI formed in the sulfonamide-based electrolyte is higher than that formed in the carbonate-based electrolyte, which can effectively stabilize the SEI.^{44,54} Moreover, the presence of lower-valence sulfur species (S[−]/S^{2−}, Fig. S18, ESI†) could facilitate the Li⁺ transportation³⁶ and lower the Li stripping/plating overpotential. These results suggest that our sulfonamide-based electrolyte successfully stabilizes the LMA-electrolyte interface and thus enables a highly reversible LMA. Finally, compared to carbonate electrolytes, the cost of the DMCF₃SA solvent is still higher (Table S2, ESI†), which is expected to be greatly reduced if mass production is realized as the cost of organic solvents is highly scale-sensitive.

Conclusions

In the present work, we designed and demonstrated a sulfonamide-based electrolyte to stabilize the electrode–electrolyte interface in high-voltage Li metal||LCO batteries. The sulfonamide-based electrolyte successfully enables excellent cycling performance of commercial LCO cathodes with high capacity retentions of 89% and 85% after 200 and 100 cycles at high charging voltages of 4.55 V_{Li} and 4.6 V_{Li}, respectively. Our electrolyte effectively stabilizes the cathode-electrolyte interface by suppressing surface degradation, impedance growth,

and side reactions in terms of gas evolution and Co dissolution. Beyond the cathode, the sulfonamide-based electrolyte also has excellent compatibility with the lithium metal anode featuring a high Li stripping/plating CE ~99.7% due to the formation of favorable deposition morphology and stable SEI. Our work proposes a promising strategy for designing new electrolytes to realize high-voltage and high-energy Li metal||LCO batteries.

Experimental section

Materials

LiCoO₂ (A-LCO, the LCO powder was from BTR New Energy according to the provider) cathodes were provided by Argonne National Laboratory with ~13 mg cm^{−2} active material loading. The other two types of LiCoO₂ powder used in this work were purchased from Sigma Aldrich (S-LCO) and Targray Co. Ltd (T-LCO) respectively. All the LCO powders and cathode were used without further treatment. The DMCF₃SA solvent was synthesized according to our previous work.³⁷ The LiFSI salt was provided by KISCO Co. Ltd. “m” stands for molality, mol-salt in kg-solvent (mol kg^{−1}). Certain amounts of DMCF₃SA solvent and LiFSI salt were added into a glass vial with a magnetic bar stirring for 30 min until a clear solution was obtained. All solvents needed to be purified by the 4 Å molecular sieve before use. The reference carbonate electrolyte, 1.2 M and 1 M (“M”, mol-salt in L-solution, mol L^{−1}) LiPF₆ in ethylene



carbonate (EC)/ethyl methyl carbonate (EMC) (3 : 7 wt%), were purchased from Gotion Co.

Electrochemical measurements

The S-LCO and T-LCO cathodes were fabricated by mixing LiCoO₂ powder, Super C65 (conductive agent), and polyvinylidene fluoride (PVDF, binder) with a weight ratio of 94 : 3 : 3 with *N*-methyl-2-pyrrolidone (NMP) as solvent. Then the slurry was tape-casted by doctor blade on aluminum foil followed by vacuum drying at 120 °C overnight. The obtained electrodes were punched into disks with a diameter of 10 mm and then rolled. The active material loadings of the S-LCO and T-LCO electrodes were ~4 and ~11 mg cm⁻², respectively. CR2032 coin cells with Li metal as an anode were used to evaluate the electrochemical performance. Electrolytes were injected by pipette to control the electrolyte amount (sulfonamide-based electrolyte: 15 µL per cell and carbonate-based electrolyte: 50 µL per cell). 350 µm-thick Li metal foils were used. The cells were tested by the galvanostatic method with different current densities on Landt CT 2001A and BTS9000 Neware cyclers. A well-established method⁵⁵ was used to evaluate the Li-metal stripping/plating Coulombic efficiency. In detail, 4 mA h cm⁻² Li was firstly plated onto the Cu substrate, followed by fully stripping to 1.5 V_{Li} to remove possible oxidation layer. Subsequently, 4 mA h cm⁻² Li was redeposited at 0.2 mA cm⁻² as a Li reservoir, then 0.5 mA h cm⁻² Li was stripped and plated at a current density of 0.5 mA cm⁻² between Li and Cu for 10 cycles. After that, the remaining Li reservoir was fully stripped at 0.4 mA cm⁻². The galvanostatic intermittent titration technique (GITT) was conducted to evaluate the overpotentials after cycling with current pulse intervals at 20 mA g⁻¹ for 8 minutes and rests for 60 minutes after each pulse. Linear sweeping voltammetry (LSV) was used to measure the electrochemical stability window of the electrolytes with Li||Al (coated with Super C65 and PVDF) configuration at a scanning rate of 4 mV s⁻¹. An anode-free cell was constructed using A-LCO as the cathode, bare Cu as an anode, and 1 m LiFSI/DMCF₃SA as an electrolyte. The A-LCO cathode loading is 2.5 mA h cm⁻², and the electrolyte/capacity ratio (E/C ratio) is 3.2 g A h⁻¹. The cell was tested by a galvanostatic method with C/5 charging and C/2 discharging (C/10 charging-discharging for the initial 3 cycles) between 3 and 4.5 V at room temperature.

Characterization

The cycled Li||LCO cells with different electrolytes were disassembled in a glovebox filled with Ar, followed by washing with dimethyl ether (DME, for Li anode) and dimethyl carbonate (DMC, for LCO cathodes) three times to remove residual lithium salts. Scanning electron microscopy (SEM, Zeiss Merlin) coupled with energy-dispersive spectroscopy (EDS) was performed to examine the surface morphology and identify the elemental compositions. Focused ion beam (FIB, NVision 40 CrossBeam, ZEISS Co.) was used to prepare thin slices for transmission electron microscopy (TEM) and cross-sectional SEM observations. *In situ* differential electrochemistry mass spectrometry (DEMS) was conducted to detect the gas

species during cell operation. *Ex situ* transmission X-ray microscopy X-ray absorption near-edge structure (TXM XANES) was performed to map the Co oxidation states of the LCO electrodes cycled in different electrolytes after charging to 4.55 V_{Li} at the full-field X-ray imaging (FXI) beamline at NSLS II of Brookhaven National Laboratory. The TXM results were analyzed by a whiteline peak position tracking method.⁴⁸ Soft X-ray absorption spectroscopy (sXAS) measurements in total electron yield (TEY) and partial fluorescence yield (PFY) detection modes were conducted at the IOS beamline (23-ID-2) of the National Synchrotron Light Source II (NSLS-II), Brookhaven National Laboratory. Samples at discharged states were mounted on a sample plate using carbon tape and loaded into the ultrahigh vacuum (UHV) chamber before measurement. PFY spectra were measured using a Vortex EM silicon drift detector. X-ray diffraction (XRD, Rigaku SmartLab) was conducted on pristine and cycled LCO cathodes for phase identification and peak intensity ratios were calculated by the ratio of peak areas after background subtraction. *In situ* Fourier-transform infrared spectroscopy (FT-IR) was performed by a specially designed electrochemical cell to characterize the evolution of CEIs during galvanostatic charging to 4.8 V_{Li} at a current density of 25 mA g⁻¹. More details about *in situ* FT-IR can be found in our previous work.¹² FT-IR spectra were also acquired at regular intervals during holding the potential at 4.8 V_{Li} and subsequent resting at open circuit potential. An *ex situ* X-ray photoelectron spectrometer (XPS, Physical Electronics Versaprobe II) was used to analyze the surface chemistry of the cycled electrodes and carbon-free, binder-free electrodes at different states of charge. Samples were transferred by a specially designed transfer vessel to avoid any contact with air. The carbon-free, binder-free electrodes were fabricated by mixing LCO powder with NMP in a 1 : 50 mass ratio. The slurry was cast on a piece of aluminum foil followed by vacuum drying at 120 °C overnight. The obtained LCO electrodes were then roll-pressed and punched. Half cells were assembled with the carbon-free, binder-free electrodes and were then charged to 4.2, 4.4, 4.5, 4.6, and 4.7 V_{Li} at a rate of 1/20 C. *Ex situ* XPS spectra on carbon-free and binder-free electrodes were normalized for comparison.

First-principles calculations

DFT, as implemented in the VASP package⁵⁶ was employed in this study, with the projector augmented wave method⁵⁷ and Perdew–Burke–Ernzerhof⁵⁸ exchange–correlation functional. The energy cutoff used is 500 eV, and a 1 × 1 × 1 Monkhorst–Pack⁵⁹ *k*-point sampling is adopted. We took the literature values⁴⁴ ($U_{\text{eff}} = 6.7$ eV and $J = 1$ eV) for the DFT+U treatment of Co 3d orbitals. DFT-D3 correction⁶⁰ was also used to account for the van der Waals effect. To simulate the LCO surface, a 4 × 4 × 1 slab with 20 Å vacuum was built, and atoms in the bottom 4.8 Å were kept immobile during ionic relaxations. The reaction on the LCO surface includes H-abstraction and C–O bond formation between the solvent and the LCO. The overall reaction energy (ΔE) was therefore computed as the difference between the energy of the eventual



adsorbate-LCO system (E_{adsorbed}) and the sum of independent solvent molecule (E_{solvent}) and a clean LCO substrate ($E_{\text{substrate}}$): $\Delta E \equiv E_{\text{adsorbed}} - (E_{\text{solvent}} + E_{\text{substrate}})$. Here, a less negative value implies higher oxidation resistance of the solvent molecule.

Conflicts of interest

There are no conflicts to declare.

Acknowledgements

J. L. acknowledges support by Honda Research Institute and NSF CBET-2034902. The authors acknowledge the cathodes provided by US DOE CAMP Facility, Argonne National Laboratory, and LiFSI salt by KISCO Co. Ltd. This work made use of the MRSEC Shared Experimental Facilities supported by the National Science Foundation under award number DMR-1419807. This work used resources of the beamlines FXI (18-ID) and IOS (23-ID-2) of the National Synchrotron Light Source II, a U.S. Department of Energy (DOE) Office of Science User Facility operated for the DOE Office of Science by Brookhaven National Laboratory under Contract No. DE-SC0012704.

References

- 1 R. Schmuck, R. Wagner, G. Hörpel, T. Placke and M. Winter, *Nat. Energy*, 2018, **3**, 267–278.
- 2 W. Xue, Z. Shi, L. Suo, C. Wang, Z. Wang, H. Wang, K. P. So, A. Maurano, D. Yu, Y. Chen, L. Qie, Z. Zhu, G. Xu, J. Kong and J. Li, *Nat. Energy*, 2019, **4**, 374–382.
- 3 W. Xue, L. Miao, L. Qie, C. Wang, S. Li, J. Wang and J. Li, *Curr. Opin. Electrochem.*, 2017, **6**, 92–99.
- 4 J. Liu, Z. Bao, Y. Cui, E. J. Dufek, J. B. Goodenough, P. Khalifah, Q. Li, B. Y. Liaw, P. Liu, A. Manthiram, Y. S. Meng, V. R. Subramanian, M. F. Toney, V. V. Viswanathan, M. S. Whittingham, J. Xiao, W. Xu, J. Yang, X.-Q. Yang and J.-G. Zhang, *Nat. Energy*, 2019, **4**, 180–186.
- 5 S. Kalluri, M. Yoon, M. Jo, S. Park, S. Myeong, J. Kim, S. X. Dou, Z. Guo and J. Cho, *Adv. Energy Mater.*, 2017, **7**, 1601507.
- 6 X. Wang, X. Wang and Y. Lu, *Ind. Eng. Chem. Res.*, 2019, **58**, 10119–10139.
- 7 Q. Liu, X. Su, D. Lei, Y. Qin, J. Wen, F. Guo, Y. A. Wu, Y. Rong, R. Kou, X. Xiao, F. Aguesse, J. Bareño, Y. Ren, W. Lu and Y. Li, *Nat. Energy*, 2018, **3**, 936–943.
- 8 Y. Huang, Y. Zhu, H. Fu, M. Ou, C. Hu, S. Yu, Z. Hu, C.-T. Chen, G. Jiang, H. Gu, H. Lin, W. Luo and Y. Huang, *Angew. Chem., Int. Ed.*, 2020, **60**, 4682–4688.
- 9 Z. Zhu, D. Yu, Z. Shi, R. Gao, X. Xiao, I. Waluyo, M. Ge, Y. Dong, W. Xue, G. Xu, W.-K. Lee, A. Hunt and J. Li, *Energy Environ. Sci.*, 2020, **13**, 1865–1878.
- 10 Z. Zhu, D. Yu, Y. Yang, C. Su, Y. Huang, Y. Dong, I. Waluyo, B. Wang, A. Hunt and X. Yao, *Nat. Energy*, 2019, **4**, 1049–1058.
- 11 J. G. Han, K. Kim, Y. Lee and N. S. Choi, *Adv. Mater.*, 2019, **31**, e1804822.
- 12 Y. Zhang, Y. Katayama, R. Tatara, L. Giordano, Y. Yu, D. Fraggedakis, J. G. Sun, F. Maglia, R. Jung and M. Z. Bazant, *Energy Environ. Sci.*, 2020, **13**, 183–199.
- 13 Y. Yu, P. Karayaylali, Y. Katayama, L. Giordano, M. Gauthier, F. Maglia, R. Jung, I. Lund and Y. Shao-Horn, *J. Phys. Chem. C*, 2018, **122**, 27368–27382.
- 14 M. Gauthier, T. J. Carney, A. Grimaud, L. Giordano, N. Pour, H. H. Chang, D. P. Fenning, S. F. Lux, O. Paschos, C. Bauer, F. Maglia, S. Lupart, P. Lamp and Y. Shao-Horn, *J. Phys. Chem. Lett.*, 2015, **6**, 4653–4672.
- 15 J. Qian, L. Liu, J. Yang, S. Li, X. Wang, H. L. Zhuang and Y. Lu, *Nat. Commun.*, 2018, **9**, 4918.
- 16 K. Wang, J. Wan, Y. Xiang, J. Zhu, Q. Leng, M. Wang, L. Xu and Y. Yang, *J. Power Sources*, 2020, **460**, 228062.
- 17 Z. Zhu, H. Wang, Y. Li, R. Gao, X. Xiao, Q. Yu, C. Wang, I. Waluyo, J. Ding, A. Hunt and J. Li, *Adv. Mater.*, 2020, **32**, 2005182.
- 18 J.-N. Zhang, Q. Li, C. Ouyang, X. Yu, M. Ge, X. Huang, E. Hu, C. Ma, S. Li, R. Xiao, W. Yang, Y. Chu, Y. Liu, H. Yu, X.-Q. Yang, X. Huang, L. Chen and H. Li, *Nat. Energy*, 2019, **4**, 594–603.
- 19 X. Yang, M. Lin, G. Zheng, J. Wu, X. Wang, F. Ren, W. Zhang, Y. Liao, W. Zhao, Z. Zhang, N. Xu, W. Yang and Y. Yang, *Adv. Funct. Mater.*, 2020, **30**, 2004664.
- 20 M. Yoon, Y. Dong, Y. Yoo, S. Myeong, J. Hwang, J. Kim, S. H. Choi, J. Sung, S. J. Kang, J. Li and J. Cho, *Adv. Funct. Mater.*, 2019, **30**, 1907903.
- 21 Z. Li, A. Li, H. Zhang, F. Ning, W. Li, A. Zangiabadi, Q. Cheng, J. J. Borovilas, Y. Chen, H. Zhang, X. Xiao, C. Ouyang, X. Huang, W.-K. Lee, M. Ge, Y. S. Chu, X. Chuan and Y. Yang, *Energy Storage Mater.*, 2020, **29**, 71–77.
- 22 K. Nie, X. Sun, J. Wang, Y. Wang, W. Qi, D. Xiao, J.-N. Zhang, R. Xiao, X. Yu, H. Li, X. Huang and L. Chen, *J. Power Sources*, 2020, **470**, 228423.
- 23 Y. Wang, Q. Zhang, Z. C. Xue, L. Yang, J. Wang, F. Meng, Q. Li, H. Pan, J. N. Zhang, Z. Jiang, W. Yang, X. Yu, L. Gu and H. Li, *Adv. Energy Mater.*, 2020, **10**, 2001413.
- 24 X. Ren, X. Zhang, Z. Shadike, L. Zou, H. Jia, X. Cao, M. H. Engelhard, B. E. Matthews, C. Wang, B. W. Arey, X. Q. Yang, J. Liu, J. G. Zhang and W. Xu, *Adv. Mater.*, 2020, **32**, 2004898.
- 25 S. Lin and J. Zhao, *ACS Appl. Mater. Interfaces*, 2020, **12**, 8316–8323.
- 26 T. Dong, J. Zhang, G. Xu, J. Chai, H. Du, L. Wang, H. Wen, X. Zang, A. Du, Q. Jia, X. Zhou and G. Cui, *Energy Environ. Sci.*, 2018, **11**, 1197–1203.
- 27 M. Zhang, J. Zhang, J. Yang, X. Du, Z. Chen, K. Chen, C. Lu, H. Zhang, T. Dong, J. Li, Z. Zhang, H. Zhang and G. Cui, *J. Electrochem. Soc.*, 2019, **166**, A2313–A2321.
- 28 M. Zhao, X. Zuo, X. Ma, X. Xiao, L. Yu and J. Nan, *J. Power Sources*, 2016, **323**, 29–36.
- 29 C. Pang, G. Xu, W. An, G. Ding, X. Liu, J. Chai, J. Ma, H. Liu and G. Cui, *Energy Technol.*, 2017, **5**, 1979–1989.

30 L. Wang, B. Chen, J. Ma, G. Cui and L. Chen, *Chem. Soc. Rev.*, 2018, **47**, 6505–6602.

31 H. Sun, G. Zhu, Y. Zhu, M. C. Lin, H. Chen, Y. Y. Li, W. H. Hung, B. Zhou, X. Wang, Y. Bai, M. Gu, C. L. Huang, H. C. Tai, X. Xu, M. Angell, J. J. Shyue and H. Dai, *Adv. Mater.*, 2020, **32**, 2001741.

32 T. Li, X.-Q. Zhang, P. Shi and Q. Zhang, *Joule*, 2019, **3**, 2647–2661.

33 Z. Yu, H. Wang, X. Kong, W. Huang, Y. Tsao, D. G. Mackanic, K. Wang, X. Wang, W. Huang, S. Choudhury, Y. Zheng, C. V. Amanchukwu, S. T. Hung, Y. Ma, E. G. Lomeli, J. Qin, Y. Cui and Z. Bao, *Nat. Energy*, 2020, **5**, 526–533.

34 R. Weber, M. Genovese, A. J. Louli, S. Hames, C. Martin, I. G. Hill and J. R. Dahn, *Nat. Energy*, 2019, **4**, 683–689.

35 H. Yang, J. Li, Z. Sun, R. Fang, D.-W. Wang, K. He, H.-M. Cheng and F. Li, *Energy Storage Mater.*, 2020, **30**, 113–129.

36 W. Xue, Z. Shi, M. Huang, S. Feng, C. Wang, F. Wang, J. Lopez, B. Qiao, G. Xu, W. Zhang, Y. Dong, R. Gao, Y. Shao-Horn, J. A. Johnson and J. Li, *Energy Environ. Sci.*, 2020, **13**, 212–220.

37 S. Feng, M. Huang, J. R. Lamb, W. Zhang, R. Tatara, Y. Zhang, Y. Guang Zhu, C. F. Perkins, J. A. Johnson and Y. Shao-Horn, *Chem*, 2019, **5**, 2630–2641.

38 A. Shyamsunder, W. Beichel, P. Klose, Q. Pang, H. Scherer, A. Hoffmann, G. K. Murphy, I. Krossing and L. F. Nazar, *Angew. Chem., Int. Ed.*, 2017, **56**, 6192–6197.

39 W. Xue, M. Huang, Y. Li, Y. G. Zhu, R. Gao, X. Xiao, W. Zhang, S. Li, G. Xu and Y. Yu, *Nat. Energy*, 2021, **6**, 495–505.

40 L. Giordano, P. Karayaylali, Y. Yu, Y. Katayama, F. Maglia, S. Lux and Y. Shao-Horn, *J. Phys. Chem. Lett.*, 2017, **8**, 3881–3887.

41 L. Giordano, T. M. Østergaard, S. Muy, Y. Yu, N. Charles, S. Kim, Y. Zhang, F. Maglia, R. Jung and I. Lund, *Chem. Mater.*, 2019, **31**, 5464–5474.

42 E. Trevisanello, R. Ruess, G. Conforto, F. H. Richter and J. Janek, *Adv. Energy Mater.*, 2021, **11**, 2003400.

43 L. Giordano, P. Karayaylali, Y. Yu, Y. Katayama, F. Maglia, S. Lux and Y. Shao-Horn, *J. Phys. Chem. Lett.*, 2017, **8**, 3881–3887.

44 X. Fan, L. Chen, O. Borodin, X. Ji, J. Chen, S. Hou, T. Deng, J. Zheng, C. Yang, S.-C. Liou, K. Amine, K. Xu and C. Wang, *Nat. Nanotechnol.*, 2018, **13**, 715–722.

45 T. M. Østergaard, L. Giordano, I. E. Castelli, F. Maglia, B. K. Antonopoulos, Y. Shao-Horn and J. Rossmeisl, *J. Phys. Chem. C*, 2018, **122**, 10442–10449.

46 Z. Chen and J. R. Dahn, *Electrochem. Solid-State Lett.*, 2004, **7**, A11.

47 J. Li, C. Lin, M. Weng, Y. Qiu, P. Chen, K. Yang, W. Huang, Y. Hong, J. Li, M. Zhang, C. Dong, W. Zhao, Z. Xu, X. Wang, K. Xu, J. Sun and F. Pan, *Nat. Nanotechnol.*, 2021, **16**, 599–605.

48 M. Wolf, B. M. May and J. Cabana, *Chem. Mater.*, 2017, **29**, 3347–3362.

49 Y. Wang, E. Wang, X. Zhang and H. Yu, *Energy Fuels*, 2021, **35**, 1918–1932.

50 F. Zhang, S. Lou, S. Li, Z. Yu, Q. Liu, A. Dai, C. Cao, M. F. Toney, M. Ge, X. Xiao, W. K. Lee, Y. Yao, J. Deng, T. Liu, Y. Tang, G. Yin, J. Lu, D. Su and J. Wang, *Nat. Commun.*, 2020, **11**, 3050.

51 A. Yano, M. Shikano, A. Ueda, H. Sakaue and Z. Ogumi, *J. Electrochem. Soc.*, 2016, **164**, A6116–A6122.

52 X. Ren, L. Zou, X. Cao, M. H. Engelhard, W. Liu, S. D. Burton, H. Lee, C. Niu, B. E. Matthews, Z. Zhu, C. Wang, B. W. Arey, J. Xiao, J. Liu, J.-G. Zhang and W. Xu, *Joule*, 2019, **3**, 1662–1676.

53 X. Cao, X. Ren, L. Zou, M. H. Engelhard, W. Huang, H. Wang, B. E. Matthews, H. Lee, C. Niu, B. W. Arey, Y. Cui, C. Wang, J. Xiao, J. Liu, W. Xu and J.-G. Zhang, *Nat. Energy*, 2019, **4**, 796–805.

54 L. Suo, W. Xue, M. Gobet, S. G. Greenbaum, C. Wang, Y. Chen, W. Yang, Y. Li and J. Li, *Proc. Natl. Acad. Sci. U. S. A.*, 2018, **115**, 1156–1161.

55 B. D. Adams, J. Zheng, X. Ren, W. Xu and J.-G. Zhang, *Adv. Energy Mater.*, 2017, **8**, 1702097.

56 G. Kresse and J. Furthmüller, *Phys. Rev. B: Condens. Matter Mater. Phys.*, 1996, **54**, 11169.

57 P. E. Blöchl, *Phys. Rev. B: Condens. Matter Mater. Phys.*, 1994, **50**, 17953.

58 J. P. Perdew, K. Burke and M. Ernzerhof, *Phys. Rev. Lett.*, 1996, **77**, 3865.

59 H. J. Monkhorst and J. D. Pack, *Phys. Rev. B: Solid State*, 1976, **13**, 5188.

60 S. Grimme, J. Antony, S. Ehrlich and H. Krieg, *J. Chem. Phys.*, 2010, **132**, 154104.

